Computer Modeling in Engineering & Sciences

Tech Science Press

DOI: 10.32604/cmes.2023.029565

ARTICLE

Outage Probability Analysis for D2D-Enabled Heterogeneous Cellular Networks with Exclusion Zone: A Stochastic Geometry Approach

Yulei Wang[1], Li Feng[1,*], Shumin Yao[1,2], Hong Liang[1], Haoxu Shi[1] and Yuqiang Chen[3]

[1]School of Computer Science and Engineering, Macau University of Science and Technology, Taipa, Macau, China

[2]Department of Broadband Communication, Peng Cheng Laboratory, Shenzhen, China

[3]School of Artificial Intelligence, Dongguan Polytechnic, Dongguan, China

*Corresponding Author: Li Feng. Email: lfeng@must.edu.mo

Received: 27 February 2023 Accepted: 08 May 2023 Published: 22 September 2023

ABSTRACT

Interference management is one of the most important issues in the device-to-device (D2D)-enabled heterogeneous cellular networks (HetCNets) due to the coexistence of massive cellular and D2D devices in which D2D devices reuse the cellular spectrum. To alleviate the interference, an efficient interference management way is to set exclusion zones around the cellular receivers. In this paper, we adopt a stochastic geometry approach to analyze the outage probabilities of cellular and D2D users in the D2D-enabled HetCNets. The main difficulties contain three aspects: 1) how to model the location randomness of base stations, cellular and D2D users in practical networks; 2) how to capture the randomness and interrelation of cellular and D2D transmissions due to the existence of random exclusion zones; 3) how to characterize the different types of interference and their impacts on the outage probabilities of cellular and D2D users. We then run extensive Monte-Carlo simulations which manifest that our theoretical model is very accurate.

KEYWORDS

Device-to-device (D2D)-enabled heterogeneous cellular networks (HetCNets); exclusion zone; stochastic geometry (SG); Matérn hard-core process (MHCP)

1 Introduction

As the number of wireless connected devices grows explosively in the upcoming sixth generation (6G) era [1,2], it can be foreseen that heterogeneous cellular (i.e., smartphones) and device-to-device (i.e., wearable devices) devices will densely coexist to extensively collect and frequently exchange information [3] and have widespread application prospects in many fields [4,5]. In the device-to-device (D2D)-enabled heterogeneous cellular networks (HetCNets) [6,7], D2D devices reuse the cellular spectrum, which may result in severe interference for the reception of cellular signals at the base stations (BSs). To alleviate the interference, an efficient interference management way is to set exclusion zones around the receivers [8–10]. That is, when a BS is receiving desired signals from cellular devices, the exclusion zone, defined as a cycle region, centered at the BS is set, in which the D2D devices are inhibited to perform any transmissions.

1.1 Motivation

Whether the information can be successfully transmitted is an important performance metric for wireless devices. In this paper, we aim to theoretically analyze the outage probabilities (i.e., unsuccessful transmission probabilities) of cellular and D2D devices in D2D-enabled HetCNets with exclusion zone. However, we are facing the following major difficulties. First, in practical network deployment, cellular and D2D devices are randomly located in the space, while BSs are deployed with strict requirements and restrictions, the two facts affect the outage probabilities greatly. It is difficult to model the location randomness of BSs, cellular and D2D devices in practice. Second, cellular transmissions occur randomly, leading to random exclusion zones around the BS receivers, further leading to random D2D transmissions. It is difficult to capture the randomness and interrelation of cellular and D2D transmissions. Third, different types of cellular and D2D devices perform transmissions concurrently; they mutually interfere with each other. It is difficult to characterize the different types of interference and their impacts on the outage probabilities of cellular and D2D devices. The above three difficulties motivate this study.

1.2 Contributions

Consider a D2D-enabled HetCNet with exclusion-zone, we theoretically analyze the outage probabilities of cellular and D2D devices and make the following novel contributions:

- We adopt a stochastic geometry (SG) approach to solve the abovementioned three difficulties. To address difficulty 1, we use Matérn hard-core process (MHCP) to model the real location distribution of BSs and use homogeneous Poisson point processes (HPPPs) to capture the location randomness of cellular and D2D devices in practical networks. To address difficulty 2, we first model the transmitting cellular devices by a thinned HPPP, and then model the activated D2D devices outside the exclusion zones by Poisson hole process (PHP). To address difficulty 3, we characterize mutual interference among the concurrent cellular and D2D transmissions by approximating MHCP of receiving BSs and PHP of activated D2D devices with PPPs and further estimating the intensities of different types of transmitting cellular and D2D devices.
- With our model, we theoretically analyze the outage probabilities of cellular and D2D devices, which are formulated as functions of system parameters, including the intensities of transmitting cellular and D2D devices, the minimum distance among BSs, and the radius of exclusion zones around BSs.
- We verify the accuracy of our theoretical model via extensive Monte-Carlo simulations.

The rest paper is organized as follows. Section 2 presents the related work. Section 3 introduces some stochastic geometry preliminaries. Section 4 specifies the system model of a D2D-enabled HetCNet with exclusion zone. Section 5 theoretically analyzes the outage probabilities of cellular and D2D devices with SG approach. Section 6 verifies the accuracy of our theoretical model via extensive Monte-Carlo simulations. Finally, Section 7 concludes the paper. For the ease of reference, Table 1 lists the main notations and their meanings.

Table 1: Notions and their meanings

Notation	Description	Type
$\Phi_b^0(\lambda_b^0)$	The HPPP of BSs with intensity λ_b^0 that forms the MHCP of BSs	

(Continued)

Table 1 (continued)

Notation	Description	Type
$\Phi_b^{Mk}(\lambda_b^{Mk})$	The MHCP of type k of BSs with intensity λ_b^{Mk}, where $k = \{1, 2\}$	
$\Phi_b^{Mk'}(\lambda_b^{Mk})$	The approximated PPP of BSs with intensity λ_b^{Mk}	
$\Phi_b^r(\lambda_b^r)$	The PPP of receiving BSs with intensity λ_b^r	
R_b	The minimum distance among any two BSs	BS
d_b	The radius of exclusion zone of each BS	
p_b^r	The receiving probability of each BS	
S_b	The received desired signal power from CU at BS	
I_b^*	The suffered interference at BS from $*$ (i.e., transmitting CUs, HD/FD DUs)	
$SINR_b$	The signal-to-interference-plus-noise ratio (SINR) at the BS	
$\Phi_c(\lambda_c)$	The HPPP of CUs with intensity λ_c	
$\Phi_c^t(\lambda_c^t)$	The HPPP of transmitting CUs with intensity λ_c^t	
$\mathbb{P}_c$	The outage probability of CU	
P_c	The transmission power of each CU	CU
p_c^t	The transmission probability of each CU	
$R_c/f_{R_c}(r_c)$	The transmission distance from CU to BS and its PDF	
$\Phi_d(\lambda_d)$	The HPPP of DUs with intensity λ_d	
$\Phi_d^a(\lambda_d^a)$	The PHP of activated DUs with intensity λ_d^a	
$\Phi_d^{a'}(\lambda_d^a)$	The approximated PPP of activated DUs with intensity λ_d^a	
$\Phi_H/\Phi_F(\lambda_H/\lambda_F)$	The PPP of activated DUs in HD/FD with intensity λ_H/λ_F	
$\Phi_d^H/\Phi_d^F(\lambda_H^t/\lambda_F^t)$	The PPP of transmitting DUs in HD/FD with intensity λ_H^t/λ_F^t	
$\mathbb{P}_d$	The outage probability of DU	
P_d	The transmission power of each DU	DU
p_H/p_F	The probability that a DU operates in HD/FD mode	
$R_d/f_{R_d}(r_d)$	The transmission distance from DU to DU and its PDF	
κ	The self-interference cancellation factor	
S_d	The received desired signal power from DU at the DU	
I_d^*	The suffered interference at DU from $*$ (i.e., transmitting CUs, HD/FD DUs, self-interference)	
$SINR_d$	The signal-to-interference-plus-noise ratio (SINR) at the DU	
$\mathbb{E}[S_v]$	Mean area of each Voronoi cell S_v	
R_v	The radius of the approximated circular Voronoi cell S_v	
θ_{dB}/θ	The predefined SINR threshold (unit: dB/real value, no unit)	Public
H	The power fading coefficient of small-scale fading	
α	The path-loss exponent	
σ^2	Additive white Gaussian noise with variance σ^2	

2 Related Work

This section presents existing works in terms of performance analysis of D2D-enabled HetCNets by setting exclusion zones or enabling D2D devices to operate in half-/full-duplex mode.

2.1 Set Exclusion Zones

Setting exclusion zones can effectively alleviate the interference among cellular and D2D transmissions. Many existing works have studied the exclusion zones set around transmitters or receivers.

Set exclusion zones around transmitters. Chu et al. in [11] adopted SG to study energy-harvesting-based D2D communication, where they set guard zones (also called exclusion zones) around D2D transmitters to protect D2D transmissions from interference emitted from the cellular devices. Flint et al. in [12] set guard zones around first-tier transmitters in two-tier heterogeneous networks, where they consider the exclusive relationship among the first-tier transmitters and model the spatial distribution of first-tier transmitters by Poisson hard-core process (PHCP). However, we study the D2D-enabled HetCNets with SG and set exclusion zones around the receivers to protect cellular transmissions from interference by D2D transmissions.

Set exclusion zones around receivers. Hasan et al. in [8] introduced guard zone around each receiver to balance the interference and spatial reuse, but this study is for wireless ad hoc networks. Tefek et al. in [9] set two types of exclusion zones around primary receivers and secondary transmitters in two-tier cognitive networks, and analyze the transmission capacities and outage probabilities of primary and secondary users with SG approach. Chen et al. in [10] studied decentralized opportunistic access for D2D underlaid cellular networks with SG and impose cellular guard zones around the BSs where no D2D transmitters can lie in, but they do not consider the minimum distance among BSs. Different from the above works, we adopt SG to study the D2D-enabled HetCNets and consider the exclusive relationship among BSs in practical networks. Besides, D2D devices can operate in half-/full-duplex mode optionally. The performance frameworks in the above works are not suitable in our research scenario.

2.2 Operate in Half-/Full-Duplex Mode

Despite the HD mode, each DU can operate in FD mode optionally to further promote to double the spectral efficiency. Some previous works analyze the performance of HD/FD D2D transmissions.

Operate in HD mode. Huang et al. in [13] studied the energy-efficient mode selection for D2D communications in cellular networks, which enable HD D2D users to select approximated modes, and then analyze the success probability and ergodic capacity for both cellular and D2D links using SG. Sun et al. in [14] controled the transmit power for D2D transmitters based on the statistical channel-state information to mitigate interference among D2D and cellular communications in D2D-underlaid cellular networks, and adopt SG to analyze the success probability and the energy efficiency of D2D communications. In contrast, we analyze the D2D transmissions where D2D devices can operate in HD/FD mode optionally, and we employ exclusion zones around the BS receivers to alleviate the interference.

Operate in FD mode. Badri et al. in [15] and [16] studied FD D2D communication in cellular networks, which enable D2D users to optionally work in HD/FD mode to alleviate the interference and guarantee the quality of service (QoS) of the cellular users. However, they do not consider the real deployment of BSs. Different from the above works, our study captures the location randomness of BS, cellular and D2D devices in real networks, the randomness and interrelation of cellular and D2D transmissions as well as the mutual interference and characterize their impacts on the outage probabilities of cellular and D2D transmissions.

3 Stochastic Geometry Preliminaries

Stochastic geometry (SG) approach, which provides various powerful tools to model the spatial location distribution of wireless devices and characterize the interference effect, has been widely used in wireless networks [17]. Many existing works [15,16,18] adopted homogeneous Poisson point process (HPPP) to model the spatial distribution of the wireless devices, which assumes devices are independently distributed and is the most popular spatial point process owing to its mathematical tractability. However, in practical networks, the transmitters are deployed with strict requirements and restrictions in order to alleviate interference, extend coverage region and reduce deployment costs, and thus an exclusion zone among the locations of the transmitters naturally arises. In this context, hard-core point process (HCPP) [12,19,20], which forbids devices to lie closer than a certain minimum distance has drawn much attention, such as PHCP [12] or MHCP [19,20]. According to whether there is a practical exclusive relationship among devices, we assume that the D2D and cellular users follow HPPPs and assume that base stations follow MHCP in our study. Below, we briefly present some terminologies and SG tools involved in this paper. Readers can refer to [21–24] for further details.

Definition 1. (Poisson point process) A spatial point process $\Phi = \{x_i,\ i \in \mathbb{N}^+\} \subset \mathbb{R}^d$ with intensity measure $\wedge$ is a Poisson point process (PPP) [18], if the random number of points of Φ for every bounded Borel set $\mathcal{B} \subset \mathbb{R}^d$ has a Poisson distribution with mean $\wedge(\mathcal{B})$, that is,

$$\mathbb{P}[\Phi(\mathcal{B}) = k] = e^{-\wedge(\mathcal{B})}\frac{(\wedge(\mathcal{B}))^k}{k!}$$

where $\wedge(\mathcal{B})$ represents the average number of points falling in the given set $\mathcal{B}$. For an HPPP, $\wedge(\mathcal{B}) = \lambda|\mathcal{B}|$, where λ is the intensity of Φ and represents the average number of points falling in per unit area or volume, $|\mathcal{B}|$ is the Lebesgue measure (i.e., area) of set $\mathcal{B}$ in Euclidean space.

Definition 2. (Matérn hard-core process of type I) An MHCP of type I Φ_{M1} is formed from a dependent thinning of an HPPP $\Phi = \{x_i, i \in \mathbb{N}^+\} \subset \mathbb{R}^d$ with intensity λ. First, each point $x_i \in \Phi$ is marked if it has a neighbor within distance r. Then, remove all marked points. All the remaining points of Φ form an MHCP of type I Φ_{M1}. Mathematically, Φ_{M1} is described as

$$\Phi_{M1} = \left\{x_i \in \Phi\colon \forall x_j \in \Phi \text{ is not in } b(x_i, r)\right\}$$

where $b(x_i, r)$ represents a ball centered at $x_i \in \Phi$ with radius r. The intensity λ_{M1} of Φ_{M1} is given by $\lambda_{M1} = \lambda\exp\left(-\lambda\pi r^2\right)$.

Definition 3. (Matérn hard-core process of type II [25]) An MHCP of type II Φ_{M2} is formed from a dependent thinning of an HPPP $\Phi = \{x_i, i \in \mathbb{N}^+\} \subset \mathbb{R}^d$ with intensity λ. First, each point $x_i \in \Phi$ is marked independently with a random mark $M_i \in (0, 1)$. Then, a point $x_i \in \Phi$ is retained in Φ_{M2} if and only if the ball $b(x_i, r)$ does not contain any point of Φ with mark smaller than M_i. Mathematically, Φ_{M2} is described as

$$\Phi_{M2} = \left\{x_i \in \Phi\colon M_i < M_j, \forall x_j \in \Phi \cap b(x_i, r)\backslash x_i\right\}.$$

The probability that each point $x_i \in \Phi$ is retained in Φ_{M2} can be expressed as $\mathbb{P}_{M2} = \frac{1-\exp\left(-\lambda\pi r^2\right)}{\lambda\pi r^2}$ [26]. Then, the intensity λ_{M2} of Φ_{M2} is given by $\lambda_{M2} = \lambda\mathbb{P}_{M2} = \frac{1-\exp\left(-\lambda\pi r^2\right)}{\pi r^2}$, which can be further written with the intensity λ_{M1} of Φ_{M1} as $\lambda_{M2} = \frac{1}{\pi r^2}\left(1 - \frac{\lambda_{M1}}{\lambda}\right)$.

Definition 4. (Poisson hole process) Let $\Phi_1 = \{x_i, i \in \mathbb{N}^+\} \subset \mathbb{R}^d$ with intensity λ_1 and $\Phi_2 = \{y_i, i \in \mathbb{N}^+\} \subset \mathbb{R}^d$ with intensity λ_2 ($\lambda_2 \gg \lambda_1$) be two independent PPPs in a given bounded Borel set

$\mathcal{B} \subset \mathbb{R}^d$. For each point $x_i \in \Phi_1$, remove all the points $y_i \in \Phi_2$ in $b(x_i, r)$. All the removed points of Φ_2 form the Hole-0 process Φ_{h0} [27] with intensity $\lambda_{h0} = \lambda_2 \left(1 - \exp\left(-\lambda_1 \pi r^2\right)\right)$, and the remaining points of Φ_2 form the Poisson hole process (PHP) Φ_{PHP} (also named as Hole-1 process [27]) with intensity $\lambda_{PHP} = \lambda_2 \exp\left(-\lambda_1 \pi r^2\right)$.

Definition 5. (Probability generating functional) Let $\Phi = \{x_i, i \in \mathbb{N}^+\} \subset \mathbb{R}^d$ be a spatial point process with intensity measure $\wedge$, for any measurable function $f(x) : \mathbb{R}^d \to [0, 1]$, the probability generating functional (PGFL) of Φ is defined as

$$\mathbb{E}\left[\prod_{x_i \in \Phi} f(x)\right] \triangleq \exp\left(-\int_{\mathbb{R}^d} (1 - f(x)) \Lambda(dx)\right)$$

where $x_i \in \Phi$ represents the orthogonal coordinates of points in Φ. For an inhomogeneous PPP with intensity function $\lambda(x)$, the PGFL of Φ can expressed as

$$\mathbb{E}\left[\prod_{x_i \in \Phi} f(x)\right] = \exp\left(-\int_{\mathbb{R}^d} (1 - f(x)) \lambda(x) dx\right).$$

For an HPPP with intensity λ, the PGFL of Φ can expressed as

$$\mathbb{E}\left[\prod_{x_i \in \Phi} f(x)\right] = \exp\left(-\lambda \int_{\mathbb{R}^d} (1 - f(x)) dx\right).$$

We convert the above integral from orthogonal coordinates to polar coordinates, i.e.,

$$\mathbb{E}\left[\prod_{x_i \in \Phi} f(x)\right] = \exp\left(-\lambda \int_0^{\infty} \int_0^{2\pi} (1 - f(r)) d\omega r dr\right) = \exp\left(-\lambda \int_0^{2\pi} d\omega \int_0^{\infty} (1 - f(r)) r dr\right)$$

$$= \exp\left(-2\pi\lambda \int_0^{\infty} (1 - f(r)) r dr\right)$$

where $x_i = (r \sin \omega, r \cos \omega)$, ω is the polar angle and follows uniform distribution in $[0, 2\pi]$.

Definition 6. The Laplace transform (LT) $\mathcal{L}$ of random variable X is defined as

$$\mathcal{L}_X(s) = \mathbb{E}[\exp(-sX)] = \int_0^{\infty} \exp(-sx) f_X(x) dx$$

where $f_X(x)$ is the probability density function (PDF) of X.

4 System Model

This section specifies the system model of a D2D-enabled heterogeneous cellular network (HetCNet) with exclusion-zone in terms of network deployment, channel model, intensities of transmitting cellular and D2D users.

4.1 Network Deployment

We study a D2D-enabled HetCNet with exclusion-zone, which consists of multiple base stations (BSs), lots of cellular users (CUs) and D2D users (DUs), as shown in Fig. 1.

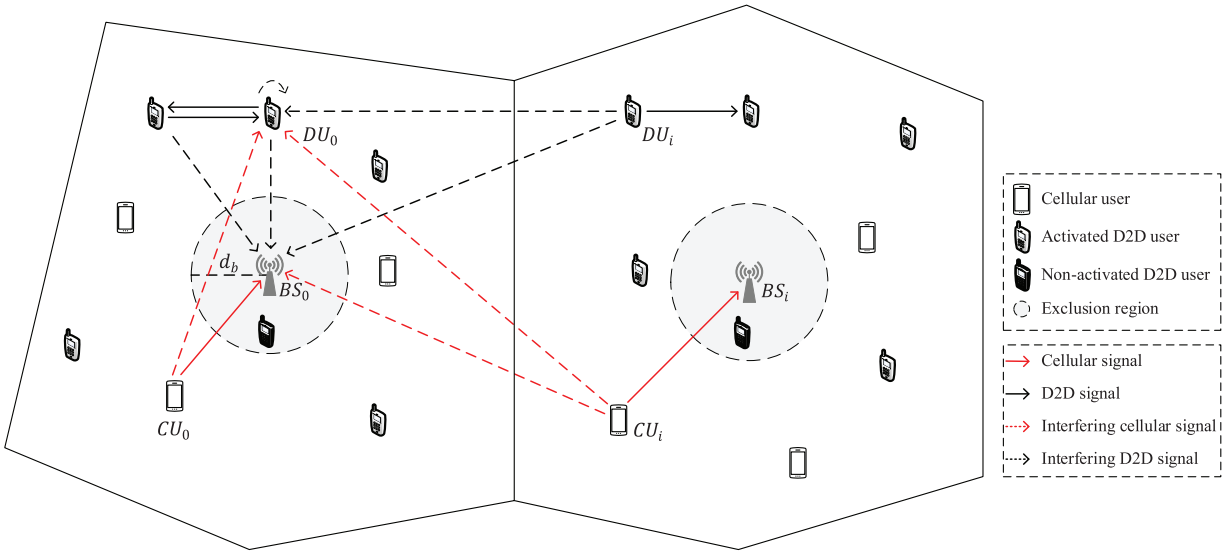

Figure 1: Overview of a D2D-enabled heterogeneous cellular network (HetCNet) with exclusion-zones around the BSs

In a typical HetCNet, the CUs and DUs are randomly located in the space, we model the locations of CUs and DUs by two independent HPPPs $\Phi_c, \Phi_d \subset \mathbb{R}^2$ with intensities λ_c and λ_d, respectively; since any two BSs cannot be arbitrarily close to each other in practical network deployment, we model the location of BSs by an MHCP of type k Φ_b^k with intensity λ_b^{Mk} $(k = \{1, 2\})$, which is formed by dependent thinning of another HPPP $\Phi_b^0 \subset \mathbb{R}^2$ with intensity λ_b^0 $(\lambda_c \gg \lambda_b^0, \lambda_d \gg \lambda_b^0)$ [19,20]. According to the definition of MHCP (i.e., Definitions 2 and 3), λ_b^{Mk} can be expressed as

$$\lambda_b^{Mk} = \begin{cases} \lambda_b^0 \exp\left(-\lambda_b^0 \pi R_b^2\right) & k = 1 \\ \dfrac{1 - \exp\left(-\lambda_b^0 \pi R_b^2\right)}{\pi R_b^2} & k = 2 \end{cases} \tag{1}$$

where R_b is the minimum distance among any two BSs.

We assume that Φ_b^0, Φ_c and Φ_d are independent, the locations of BSs, CUs and DUs are independent with each other. We assume that each CU transmits to its geographically nearest BS with a fixed power P_c, where a Voronoi tessellation is formed, as shown in Figs. 2a–2c. The mean area of each Voronoi cell S_v can be expressed as [19,21–23]

$$\mathbb{E}[S_v] = 1/\lambda_b^{Mk} \tag{2}$$

In order to facilitate the analysis, we approximate the Voronoi cell as a circle with radius R_v [28–30], i.e.,

$$R_v = \sqrt{\mathbb{E}[S_v]/\pi} = \sqrt{1/\pi\lambda_b^{Mk}} \tag{3}$$

We assume that DUs utilize the uplink cellular channel to perform D2D transmissions and may choose to operate in either HD or FD mode to transmit to its nearest DU with a fixed power P_d. When adopting FD mode, we assume the imperfect self-interference cancellation at the DU receiver side. Due to spectrum sharing, the D2D transmissions may interfere with the reception of cellular signals at the BS. To manage the interference, exclusion zones around BSs are set. In the exclusion zone centered

at each receiving BS with radius d_b, the DUs cannot be activated to perform D2D transmissions. As Figs. 1 and 2 show, DUs in the exclusion zones of BSs are non-activated; in contract, DUs outside the exclusion zones are activated.

4.2 Channel Model

We assume that all the wireless signals in D2D and cellular transmissions undergo large- and small-scale channel fading. We characterize the large-scale channel fading by the distance dependent power-law path loss model $l = \|x - y\|^{-\alpha} = R^{-\alpha}$ [31], where $R = \|x - y\|$ is Euclidean distance between a transmitter x and a receiver y, and α is the path-loss exponent which usually satisfies $2 < \alpha < 6$ [32]. We characterize the small-scale channel fading with Rayleigh fading that is modeled by an independent and identically distributed (i.i.d.) power fading coefficient H (square of the amplitude fading coefficient) [33], which follows exponential distribution with mean $1/\mu$, i.e., $H \sim Exp(\mu)$ [18]. Besides, we assume that the thermal noise at the receiver is additive white Gaussian noise with zero mean and variance σ^2 [34,35].

(a). PPP

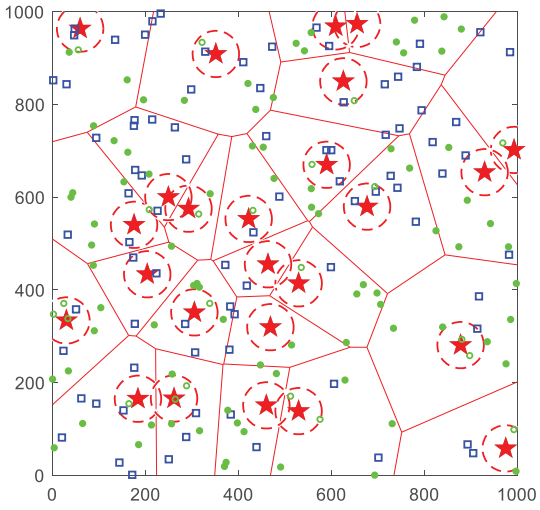

(b). MHCPP (Type I)

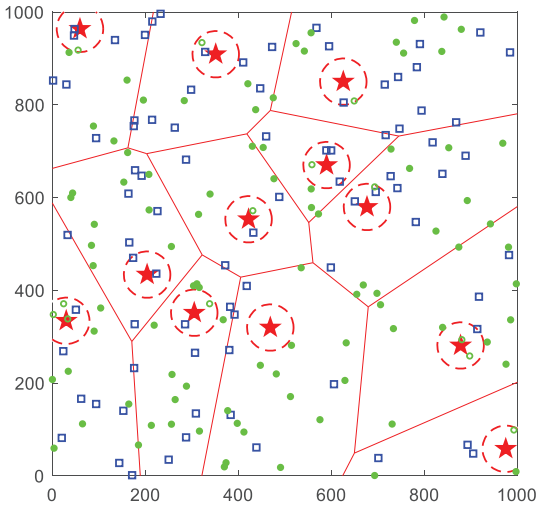

Figure 2: (Continued)

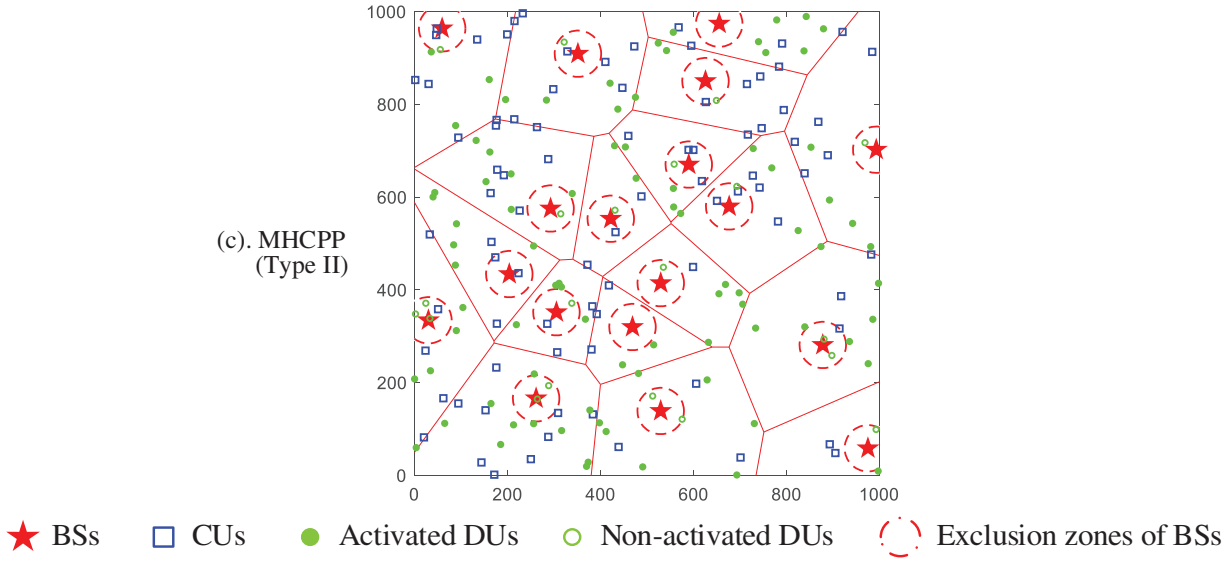

Figure 2: A snapshot of Voronoi tessellation of BSs, CUs and DUs in a 1000 m × 1000 m square region, where $\lambda_c = 100$ CUs km^{-2}, $\lambda_d = 100$ DUs km^{-2}, $R_b = 100$ m, $d_b = 50$ m. (a). BSs follow an HPPP with $\lambda_b^0 = 30$ BSs km^{-2}; (b). BSs follow an MHCP of type I with $\lambda_b^{M1} =$ BSs km^{-2}; (c). BSs follow an MHCP of type II with $\lambda_b^{M2} = 19.4$ BSs km^{-2}

4.3 Intensity of Transmitting CUs

We assume that all CUs perform ALOHA mechanism to access the channel with probability p_c^t to transmit data to its associated BSs [15]. Let Φ_c^t denote the set of transmitting CUs with intensity λ_c^t. According to independent thinning process of HPPP Φ_c, Φ_c^t is an HPPP and λ_c^t can be expressed as

$$\lambda_c^t = p_c^t \lambda_c \tag{4}$$

4.4 Intensity of Transmitting DUs

Recall that we set exclusion zones at the side of BS which is performing reception from transmitting CUs in its Voronoi cell, that is, when no CUs are transmitting in a cell, the BSs may not perform reception, the exclusion zones are not set. Let p_b^r denote the receiving probability of BSs, which is equal to the probability that there is at least a transmitting CU in a given Voronoi cell S_v. According to definition of PPP (i.e., Definition 1), p_b^r can be expressed as

$$p_b^r = 1 - \mathbb{P}\left[\Phi_c^t(S_v) = 0\right] = 1 - \exp\left(-\wedge\left(\mathbb{E}\left[S_v\right]\right)\right) \tag{5}$$

where $\wedge(\mathbb{E}[S_v])$ is the intensity measure of Φ_c^t and can be expressed as

$$\wedge\left(\mathbb{E}\left[S_v\right]\right) = \lambda_c^t \mathbb{E}\left[S_v\right] = \lambda_c^t / \lambda_b^{Mk} \tag{6}$$

Let Φ_b^r denote the set of receiving BSs with intensity λ_b^r. Due to the non-availability of any known PGFL for MHCP, for the ease of analysis, we use a PPP $\Phi_b^{Mk'}$ with same intensity λ_b^{Mk} to approximate the MHCP Φ_b^{Mk} of receiving BSs[1] [20,36–38], and the accuracy of such approximation is also validated in [39]. According to independent thinning of $\Phi_b^{Mk'}$, Φ_b^r is a PPP and λ_b^r can be expressed as

[1]The approximated PPP is inhomogeneous with constant positive density.

$$\lambda_b^r = p_b^r \lambda_b^{Mk} \tag{7}$$

Let Ξ_{d_b} denote the union of exclusion zones formed by all receiving BSs. Since each receiving BS form an exclusion zone, Ξ_{d_b} can be expressed as

$$\Xi_{d_b} \triangleq \bigcup_{y_i \in \Phi_b^r} b\left(y_i, d_b\right) \tag{8}$$

where $b\left(y_i, d_b\right)$ is an exclusion zone centered at $y_i \in \Phi_b^r$ with radius d_b.

In Ξ_{d_b}, the DUs cannot be activated to perform D2D transmissions. According to the definition of PHP (i.e., Definition 4), for the two PPPs of receiving BSs Φ_b^r and DUs Φ_d, the activated DUs outside the exclusion zones (i.e., Ξ_{d_b}) naturally form a PHP Φ_d^a with intensity λ_d^a, i.e.,

$$\lambda_d^a = \lambda_d \exp\left(-\lambda_b^r \pi d_b^2\right) \tag{9}$$

Recall that the DUs can choose to operate in either HD or FD mode [15]. We assume that a DU operates in HD and FD with probability p_H and p_F, respectively, such that $p_H + p_F = 1$. Due to the non-availability of any known PGFL for PHP, for the ease of analysis, we use a PPP $\Phi_d^{a'}$ with same intensity λ_d^a to approximate the PHP Φ_d^a of activated DUs [30,40]. According to independent thinning of PPP $\Phi_d^{a'}$, $\Phi_d^{a'}$ can be regarded as the union of two independent PPPs Φ_H of activated HD DUs with intensity λ_H and Φ_F of activated FD DUs with intensity λ_F, that is, $\Phi_d^{a'} = \Phi_H \cup \Phi_F$ [15]. Hence, λ_H, λ_F can be expressed as

$$\lambda_H = p_H \lambda_d^a, \lambda_F = p_F \lambda_d^a \tag{10}$$

We assume that half of HD DUs are transmitters and half of them are receivers [15]. Hence, the transmitting HD DUs form a thinned PPP Φ_H^t with intensity $\lambda_H^t = \lambda_H/2$. Similarly, all FD DUs are transceivers at the same time. The transmitting FD DUs form a thinned PPP Φ_F^t with intensity $\lambda_F^t = \lambda_F$.

5 Outage Probability Analysis

This section theoretically analyzes the outage probabilities of CUs and DUs with stochastic geometry approach.

5.1 Outage Probability of CUs $\mathbb{P}_c$

We first analyze the outage probability of CUs. Consider a cellular transmission from a tagged CU c_0 to a tagged BS b_0 in a distance R_c. Let $SINR_b\left(R_c, I_b\right)$ denote the signal-to-interference-plus-noise ratio (SINR) between b_0 received c_0's signal power S_b and its suffered interference signal power I_b plus noise power σ^2. Hence, the $SINR_b\left(R_c, I_b\right)$ at b_0 can be expressed as

$$SINR_b\left(R_c, I_b\right) = \frac{S_b}{I_b + \sigma^2} \tag{11}$$

where σ^2 is the noise power. In Eq. (11), S_b can be expressed as

$$S_b = P_c H_c R_c^{-\alpha} \tag{12}$$

where P_c is the transmission power of CU, H_c is the power fading coefficient between c_0 and b_0.

In Eq. (11), I_b can be expressed as

$$I_b = I_b^c + I_b^H + I_b^F \tag{13}$$

where $I_b^c = \sum_{i\in\Phi_c^t\setminus\{c_0\}} P_c H_i R_i^{-\alpha}$, $I_b^H = \sum_{i\in\Phi_H^t} P_d H_i R_i^{-\alpha}$, $I_b^F = \sum_{i\in\Phi_F^t} P_d H_i R_i^{-\alpha}$ is b_0's received interference from the other transmitting CUs, HD and FD DUs, respectively. P_d is the transmission power of DU, H_i and R_i are the power fading coefficient and distance between i and b_0, respectively.

For the tagged transmitter c_0, the transmission is unsuccessful if $SINR_b(R_c, I_b)$ at d_0 is smaller than a certain SINR threshold θ[2]. Let $\mathbb{P}_c$ denote the outage probability of c_0, which is defined as the mean value of $\mathbb{P}([SINR_b(R_c, I_b)] < \theta)$, i.e.,

$$\mathbb{P}_c = \mathbb{E}_{I_b,R_c}[\mathbb{P}(SINR_b(R_c, I_b) < \theta)] = \int_0^{R_v} \mathbb{E}_{I_b}[\mathbb{P}(SINR_b(r_c, I_b) < \theta | r_c)] \cdot f_{R_c}(r_c)\, dr_c \tag{14}$$

where $f_{R_c}(r_c)$ is the probability density function (PDF) of R_c [41]. Below, we express $f_{R_c}(r_c)$ and $\mathbb{E}_{I_b}[\mathbb{P}(SINR_b(r_c, I_b) < \theta | r_c)]$ in sequence.

Let $F_{R_c}(r_c)$ denote the cumulative distribution function (CDF) of R_c. $F_{R_c}(r_c)$ can be expressed as

$$F_{R_c}(r_c) = \mathbb{P}(R_c \le r_c) = \frac{\pi r_c^2}{\pi R_v^2} = \frac{\pi r_c^2}{1/\lambda_b^{Mk}} = \pi\lambda_b^{Mk} r_c^2, \quad 0 < r_c \le R_v; \tag{15}$$

Further, $f_{R_c}(r_c)$ can be obtained by taking derivative of $F_{R_c}(r_c)$ with respect to r_c, i.e.,

$$f_{R_c}(r_c) = \frac{dF_{R_c}(r_c)}{dr_c} = 2\pi\lambda_b^{Mk} r_c, \quad 0 < r_c \le R_v; \tag{16}$$

Then, we express $\mathbb{E}_{I_b}[\mathbb{P}(SINR_b(r_c, I_b) < \theta | r_c)]$ as

$$\begin{aligned}
&\mathbb{E}_{I_b}[\mathbb{P}(SINR_b(r_c, I_b) < \theta | r_c)] = \mathbb{E}_{I_b^c, I_b^H, I_b^F}\left[\mathbb{P}\left(\frac{P_c H_c r_c^{-\alpha}}{I_b^c + I_b^H + I_b^F + \sigma^2} < \theta | r_c\right)\right] \\
&= \mathbb{E}_{I_b^c, I_b^H, I_b^F}\left[\mathbb{P}\left(H_c < \frac{\mu\theta r_c^{\alpha}}{P_c}\left(I_b^c + I_b^H + I_b^F + \sigma^2\right) | r_c\right)\right] \\
&\overset{(a)}{=} \mathbb{E}_{I_b^c, I_b^H, I_b^F}\left[1 - \exp\left(-\frac{\mu\theta r_c^{\alpha}}{P_c}\left(I_b^c + I_b^H + I_b^F + \sigma^2\right)\right)\right] \\
&= 1 - \exp\left(-s_b\sigma^2\right)\mathbb{E}_{I_b^c}\left[\exp\left(-s_b I_b^c\right)\right]\mathbb{E}_{I_b^H}\left[\exp\left(-s_b I_b^H\right)\right]\mathbb{E}_{I_b^F}\left[\exp\left(-s_b I_b^F\right)\right] \\
&\overset{(b)}{=} 1 - \exp\left(-s_b\sigma^2\right)\mathcal{L}_{I_b^c}(s_b)\,\mathcal{L}_{I_b^H}(s_b)\,\mathcal{L}_{I_b^F}(s_b)
\end{aligned} \tag{17}$$

where $\mathbb{E}_X[AX]$ is the expectation of AX with respect to X. Eq. (a) holds because H_c follows an exponential distribution with mean $1/\mu$, i.e., $H_c \sim Exp(\mu)$. According to the CDF of an exponential distribution, if $f_{H_c}(h_c) = \mu e^{-\mu h_c}$, $\mathbb{P}(H_c < h_0) = F_{H_c}(h_0) = \int_0^{h_0} \mu e^{-\mu h_c} dh_c = 1 - \exp(-\mu h_0)$. Eq. (b) follows from the definition of LT (i.e., Definition 6) of interference I_b^c, I_b^H, and I_b^F evaluated at $s_b = \frac{\mu\theta r_c^{\alpha}}{P_c}$, respectively. We express them in sequence below.

In Eq. (17), the LT of I_b^c at b_0 is given as

$$\mathcal{L}_{I_b^c}(s_b) = \exp\left(-\lambda_c^t r_c^2 \theta^{2/\alpha} \cdot \frac{2\pi^2}{\alpha\sin(2\pi/\alpha)}\right) \tag{18}$$

[2]In general, SINR is real ratio value with no unit, SINR threshold θ is given in decibel (dB), the real value (no unit) of which is given by $\theta = 10^{\theta/10}$. When comparing SINR with θ, it should be in same scale.

Proof:

$$\mathcal{L}_{I_b^c}(s_b) = \mathbb{E}_{I_b^c}\left[\exp\left(-s_b I_b^c\right)\right] = \mathbb{E}_{R_i,H_i}\left[\exp\left(-\frac{\mu\theta r_c^{\alpha}}{P_c}\sum_{i\in\Phi_c^t\setminus\{c_0\}} P_c H_i R_i^{-\alpha}\right)\right]$$

$$\overset{(a)}{=} \mathbb{E}_{R_i}\left[\mathbb{E}_{H_i}\left[\exp\left(-\sum_{i\in\Phi_c^t\setminus\{c_0\}}\mu\theta r_c^{\alpha} H_i R_i^{-\alpha}\right)\right]\right] \overset{(b)}{=} \mathbb{E}_{R_i}\left[\prod_{i\in\Phi_c^t\setminus\{c_0\}}\mathbb{E}_{H_i}\left(\exp\left(-\mu\theta r_c^{\alpha} R_i^{-\alpha} H_i\right)\right)\right]$$

$$\overset{(c)}{=} \mathbb{E}_{R_i}\left[\prod_{i\in\Phi_c^t\setminus\{c_0\}}\int_0^{\infty}\exp\left[-\mu\theta r_c^{\alpha} R_i^{-\alpha} h_i\right] f_{H_i}(h_i)\,dh_i\right]$$

$$\overset{(d)}{=} \mathbb{E}_{R_i}\left[\prod_{i\in\Phi_c^t\setminus\{c_0\}}\int_0^{\infty}\exp\left[-\mu\theta r_c^{\alpha} R_i^{-\alpha} h_i\right]\mu\exp\left(-\mu h_i\right)dh_i\right]$$

$$= \mathbb{E}_{R_i}\left[\prod_{i\in\Phi_c^t\setminus\{c_0\}}\left(\frac{\mu}{\mu+\mu\theta r_c^{\alpha} R_i^{-\alpha}}\right)\right] = \mathbb{E}_{R_i}\left[\prod_{i\in\Phi_c^t\setminus\{c_0\}}\left(\frac{1}{1+\theta r_c^{\alpha} R_i^{-\alpha}}\right)\right]$$

In the above proof, Eq. (*a*) can be obtained from the fact that R_i and H_i are mutually independent. Eq. (*b*) follows from the property of exponential distribution, i.e., $\exp\left(\sum_i h_i\right) = \prod_i \exp(h_i)$. Eq. (*c*) is due to the definition of expectation of H_i. Eq. (*d*) holds because H_i follows an exponential distribution with mean $1/\mu$[3], i.e., $f_{H_i}(h_i) = \mu e^{-\mu h_i}$. According to the PGFL (i.e., Definition 5) of PPP Φ_c^t, we can obtain

$$\mathcal{L}_{I_b^c}(s_b) \overset{(e)}{=} \exp\left(-\lambda_c^t\int_{\mathbb{R}^2}\left(1-\frac{1}{1+\theta r_c^{\alpha} r_i^{-\alpha}}\right)dr_i\right) \overset{(f)}{=} \exp\left(-2\pi\lambda_c^t\int_0^{\infty}\left(\frac{\theta r_c^{\alpha} r_i^{-\alpha}}{1+\theta r_c^{\alpha} r_i^{-\alpha}}\right)r_i dr_i\right)$$

$$= \exp\left(-2\pi\lambda_c^t\int_0^{\infty}\frac{1}{1+\frac{1}{\theta r_c^{\alpha} r_i^{-\alpha}}}r_i dr_i\right) \overset{(g)}{=} \exp\left(-2\pi\lambda_c^t\int_0^{\infty}\left(\frac{1}{1+y^{\alpha}}\right)y\left(\theta r_c^{\alpha}\right)^{2/\alpha}dy\right)$$

$$= \exp\left(-2\pi\lambda_c^t r_c^2\theta^{2/\alpha}\int_0^{\infty}\frac{y}{1+y^{\alpha}}dy\right) \overset{(h)}{=} \exp\left(-\pi\lambda_c^t r_c^2\theta^{2/\alpha}\cdot\frac{2}{\alpha}\cdot\Gamma\left(\frac{2}{\alpha}\right)\cdot\Gamma\left(1-\frac{2}{\alpha}\right)\right)$$

$$\overset{(i)}{=} \exp\left(-\lambda_c^t r_c^2\theta^{2/\alpha}\frac{2\pi^2}{\alpha\sin(2\pi/\alpha)}\right)$$

In Eq. (*e*), $\mathbb{R}^2$ is the area in which the interfering CUs locate. Eq. (*f*) converts the expression from orthogonal coordinates to polar coordinates. Eq. (*g*) follows by changing the variable $y^{\alpha} = \frac{1}{\theta r_c^{\alpha} r_i^{-\alpha}}$, i.e., $y = \frac{r_i}{r_c\theta^{\frac{1}{\alpha}}}$, hence y belongs to $(0,\infty)$. Eq. (*h*) can refer to Eq. 3.241.4 $\int_0^{\infty}\frac{x^{a-1}}{(p+qx^b)^{n+1}}dx =$

[3]In our simulation, we set $\mu = 1$, i.e., $H_i \sim Exp(1)$.

$\frac{1}{bp^{n+1}}\left(\frac{p}{q}\right)^{\frac{a}{b}} \frac{\Gamma\left(\frac{a}{b}\right)\Gamma\left(1+n-\frac{a}{b}\right)}{\Gamma(1+n)}, \left[0<\frac{a}{b}<n+1, p\neq 0, q\neq 0\right]$ of [42]. Eq. (*i*) follows from the Euler's reflection formula $\Gamma(x)\cdot\Gamma(1-x)=\frac{\pi}{\sin(\pi x)}$, where $\Gamma(x)=\int_0^\infty t^{x-1}e^{-t}dt, x>0$ is the complete gamma function.

For the special case $\alpha=4$, we have

$$\mathcal{L}_{I_b^c}(s_b)=\exp\left(-\lambda_c^t r_c^2\sqrt{\theta}\frac{\pi^2}{2\sin(\pi/2)}\right)$$

In Eq. (17), the LT of I_b^H at b_0 is given as

$$\mathcal{L}_{I_b^H}(s_b)=\exp\left(-2\pi\lambda_H^t(s_bP_b)^{2/\alpha}\int_{\frac{d_b}{r_c\theta^{1/\alpha}}}^{\infty}\frac{y}{1+y^\alpha}dy\right) \tag{19}$$

For the special case $\alpha=4$, we have

$$\mathcal{L}_{I_b^H}(s_b)=\exp\left(-2\pi\lambda_H^t\sqrt{s_bP_b}\int_{\frac{d_b}{r_c\theta^{1/4}}}^{\infty}\frac{y}{1+y^4}dy\right)\overset{(a)}{=}\exp\left(-\pi\lambda_H^t\sqrt{s_bP_b}\left(\frac{\pi}{2}-\tan^{-1}\left(\frac{d_b^2}{r_c^2\sqrt{\theta}}\right)\right)\right)$$

where (a) follows $\int_A^\infty\frac{x}{1+x^4}dx=\frac{1}{4}\left(\pi-2\tan^{-1}\left(A^2\right)\right)$.

In Eq. (17), the LT of I_b^F at b_0 is given as

$$\mathcal{L}_{I_b^F}(s_b)=\exp\left(-2\pi\lambda_F^t(s_bP_b)^{2/\alpha}\int_{\frac{d_b}{r_c\theta^{1/\alpha}}}^{\infty}\frac{y}{1+y^\alpha}dy\right) \tag{20}$$

5.2 Outage Probability of DUs $\mathbb{P}_d$

We next analyze the outage probability of DUs in HD/FD mode. Consider a D2D transmission from a tagged DU d_{t0} to the other tagged DU d_{r0} in a distance R_d. Let $SINR_d(R_d, I_d)$ denote the SINR between d_{r0} received d_{t0}'s signal power S_d and its suffered interference signal power I_d plus noise power σ^2. Hence, the $SINR_d(R_d, I_d)$ at d_{r0} can be expressed as

$$SINR_d(R_d, I_d)=\frac{S_d}{I_d+\sigma^2} \tag{21}$$

where σ^2 is the noise power. In Eq. (21), S_d can be expressed as

$$S_d=P_dH_dR_d^{-\alpha} \tag{22}$$

where P_d is the transmission power of DU, H_d is the power fading coefficient between d_{t0} and d_{r0}.

In Eq. (21), I_d can be expressed as

$$I_d=I_d^c+I_d^H+I_d^F+I_d^s \tag{23}$$

where $I_d^c=\sum_{i\in\Phi_c^t}P_cH_iR_i^{-\alpha}$, $I_d^H=\sum_{i\in\Phi_H^t\setminus\{d_{t0}\}}P_dH_iR_i^{-\alpha}$, $I_d^F=\sum_{i\in\Phi_F^t\setminus\{d_{t0}\}}P_dH_iR_i^{-\alpha}$ is d_{t0}'s received interference from the other transmitting CUs, HD and FD DUs, respectively. H_i and R_i are the power fading coefficient and distance between i and d_{r0}, respectively. Besides, $I_d^s=\kappa P_d\mathbb{1}_{FD}$ is the self-interference due to the FD D2D transmission, κ is the self-interference cancellation factor, $\mathbb{1}_{FD}$ is the

indicator function which takes value 1 representing DU operating in FD mode and 0 representing DU operating in HD mode.

For the tagged transmitter d_{t0}, the transmission is unsuccessful if $SINR_d(R_d, I_d)$ at d_{r0} is smaller than a certain SINR threshold θ. Let $\mathbb{P}_d$ denote the outage probability of d_{t0}, which is defined as the mean value of $\mathbb{P}([SINR_d(R_d, I_d)] < \theta)$, i.e.,

$$\mathbb{P}_d = \mathbb{E}_{I_d,R_d}[\mathbb{P}(SINR_d(R_d, I_d) < \theta)] = \int_0^\infty \mathbb{E}_{I_d}[\mathbb{P}(SINR_d(r_d, I_d) < \theta | r_d)] \cdot f_{R_d}(r_d)\, dr_d \tag{24}$$

where $f_{R_d}(r_d)$ is the PDF of R_d. Below, we express $f_{R_d}(r_d)$ and $\mathbb{E}_{I_d}[\mathbb{P}(SINR_d(r_d, I_d) < \theta | r_d)]$.

Recall that the DU transmits to its nearest DU. Given the tagged DU d_{r0} in the origin and a nearest distance r_d, there is no DU closer than r_d, which means that there is no DU in the disk $b(d_{r0}, r_d)$. According to the definition of PPP Φ_d^a (i.e., Definition 1), the PDF that R_d is not smaller than r_d [41] can be derived as

$$\mathbb{P}(R_d > r_d) = \mathbb{P}(No\ device\ closer\ than\ r_d) = \mathbb{P}\left[\Phi_d^a(|S_b|) = 0\right] = \exp\left(-\lambda_d^a |S_b|\right) \tag{25}$$

where $|S_b| = \pi r_d^2$ is the area of $b(d_{r0}, r_d)$.

Let $F_{R_d}(r_d)$ denote the CDF of R_d. $F_{R_d}(r_d)$ can be expressed as

$$F_{R_d}(r_d) = \mathbb{P}(R_d \le r_d) = 1 - \mathbb{P}(R_d > r_d) = 1 - \exp\left(-\lambda_d^a \pi r_d^2\right) \tag{26}$$

Further, $f_{R_d}(r_d)$ can be obtained by taking derivative of $F_{R_d}(r_d)$ with respect to r_d, i.e.,

$$f_{R_d}(r_d) = \frac{dF_{R_d}(r_d)}{dr_d} = 2\pi\lambda_d^a r_d \exp\left(-\lambda\pi r_d^2\right) \tag{27}$$

Then, we express $\mathbb{E}_{I_d}[\mathbb{P}(SINR_d(r_d, I_d) < \theta | r_d)]$ as

$$\begin{aligned}\mathbb{E}_{I_d}[\mathbb{P}(SINR_d(r_d, I_d) < \theta | r_d)] &= \mathbb{E}_{I_d^c, I_d^H, I_d^F}\left[\mathbb{P}\left(\frac{P_d H_d r_d^{-\alpha}}{I_d^c + I_d^H + I_d^F + I_d^s + \sigma^2} < \theta | r_d\right)\right] \\ &= 1 - \exp\left(-s_d\sigma^2\right)\exp\left(-s_d I_d^s\right)\mathcal{L}_{I_d^c}(s_d)\,\mathcal{L}_{I_d^H}(s_d)\,\mathcal{L}_{I_d^F}(s_d)\end{aligned} \tag{28}$$

where $\mathcal{L}_{I_d^c}(s_d)$, $\mathcal{L}_{I_d^H}(s_d)$, and $\mathcal{L}_{I_d^F}(s_d)$ are LTs of I_d^c, I_d^H, and I_d^F evaluated at $s_d = \dfrac{\mu\theta r_d^\alpha}{P_d}$, respectively. Below, we express them in sequence.

In Eq. (28), the LT of I_d^c at d_{r0} is given as

$$\mathcal{L}_{I_d^c}(s_d) = \exp\left(-\lambda_c^t (s_d P_c)^{2/\alpha} \frac{2\pi^2}{\alpha sin(2\pi/\alpha)}\right) \tag{29}$$

If a D2D pair operates in the HD mode:

In Eq. (28), the LT of I_d^H at d_{r0} is given as

$$\mathcal{L}_{I_d^H}(s_d) = \exp\left(-2\pi\lambda_H^t r_d^2 \theta^{2/\alpha} \int_{\theta^{-\frac{1}{\alpha}}}^\infty \frac{y}{1+y^\alpha} dy\right) \tag{30}$$

In Eq. (28), the LT of I_d^F at d_{r0} is given as

$$\mathcal{L}_{I_d^F}(s_d) = \exp\left(-\lambda_F^t r_d^2 \theta^{2/\alpha} \cdot \frac{2\pi^2}{\alpha \sin(2\pi/\alpha)}\right) \tag{31}$$

If a D2D pair operates in the FD mode:

In Eq. (28), the LT of I_d^H at d_{r0} is given as

$$\mathcal{L}_{I_d^H}(s_d) = \exp\left(-\lambda_H^t r_d^2 \theta^{2/\alpha} \cdot \frac{2\pi^2}{\alpha \sin(2\pi/\alpha)}\right) \tag{32}$$

In Eq. (28), the LT of I_d^F at d_{r0} is given as

$$\mathcal{L}_{I_d^F}(s_d) = \exp\left(-2\pi\lambda_F^t r_d^2 \theta^{2/\alpha} \int_{\theta^{-\frac{1}{\alpha}}}^{\infty} \frac{y}{1+y^\alpha} dy\right) \tag{33}$$

6 Model Evaluation

In this section, we validate the accuracy of our theoretical model via extensive Monte-Carlo simulations and illustrate the outage probabilities of CUs and DUs in the D2D-enabled HetCNet with exclusion-zone. Table 2 shows the parameter settings for each simulation in Figs. 3–6, respectively. In Table 2, we use pattern 'x: y: z' to represent that a parameter takes value from x to z with an increasing step of y, use pattern 'x, y' to represent that a parameter takes value x and y, respectively. For example, in first row of Table 2, '−20:10:30' means that parameter θ takes value from −20 to 30 dB with an increasing step of 10 dB, '−50, −70' means that parameter κ takes value −50 and −70 dB, respectively. In our simulations, we set the simulation region as a circular disk with radius 10^4 m. For each simulation, we run 10^4 iterations to obtain the average value. In all figures, we use labels 'ana' and 'sim' to denote the theoretical and simulation results, respectively.

Table 2: Parameters settings for simulations

Figure	θ(dB)	κ(dB)	σ^2(dBm)	R_b(m)	p_c^t	p_H	d_b (m)	α	P_d (dBm)	P_c (dBm)	$\lambda_b^0/\lambda_c/\lambda_d$ (/Km^2)
3	−20:10:30	−50	−100	100	0.5	0.5	120	3	1	10	50/50/100
4(a)	−20:10:30	−50, −70	−100	100	0.5	0.5	120	3	1	10	50/50/100
4(b)	−20:10:30	−50	−100, −50	100	0.5	0.5	120	3	1	10	50/50/100
5(a)	−5	−50	−100	50:50:300	0.2, 0.8	0.5	150	3	1	10	50/50/100
5(b)	−5	−50	−100	50:50:300	0.5	0.2, 0.8	150	3	1	10	50/50/100
6(a)	−5	−50	−100	150	0.5	0.5	0:30:150	3, 4	1	10	50/50/150
6(b)	−5	−50	−100	150	0.5	0.5	0:30:150	3	1, 5	10	50/50/150

6.1 Outage Probabilities vs. SINR Threshold in Different BSs Distributions

Here, we verify the accuracy of outage probabilities of CUs $\mathbb{P}_c$ and DUs $\mathbb{P}_d$ as the SINR threshold θ varies from −20 to 30 dB, under different BSs distributions, i.e., MHCP of types I and II (called 'type I' and 'type II' process for short), which is also compared with PPP. From Fig. 3, we have the following observations:

- Given a specific distribution of BSs, both $\mathbb{P}_c$ and $\mathbb{P}_d$ increase as θ increases. It is because the increase of θ raises the difficulty of decoding a signal from a CU or DU, respectively.
- Given θ, $\mathbb{P}_d$ (PPP) > $\mathbb{P}_d$ (type II) > $\mathbb{P}_d$ (type I) for DUs, respectively; in contrast, $\mathbb{P}_c$ (type I) > $\mathbb{P}_c$ (type II) > $\mathbb{P}_c$ (PPP) for CUs. The reasons are as follows. In different distributions of BSs, $\lambda_b^0 > \lambda_b^{M2} > \lambda_b^{M1}$. For DUs, the larger the intensity of BSs, the more the exclusion zones of BSs, the smaller the intensity of activated DUs, the larger the average transmission distance from a DU to its nearest DU, the larger the outage probability of DUs; For CUs, the larger the intensity of BSs, the smaller the average area of each Voronoi cell, the smaller the average transmission distance from CU to BS, the smaller the outage probability of CUs.

- Given θ and a specific distribution of BSs, $\mathbb{P}_d$ (FD) > $\mathbb{P}_d$ (HD). It is because FD DUs suffer more self-interference than HD DUs due to imperfect self-interference. Besides, $\mathbb{P}_d > \mathbb{P}_c$. It is because the transmission power of DUs is lower than that of CUs.

We take the example that BSs follow the type II distribution to verify the accuracy of outage probabilities of CUs $\mathbb{P}_c$ and DUs $\mathbb{P}_d$ and show the new insights below.

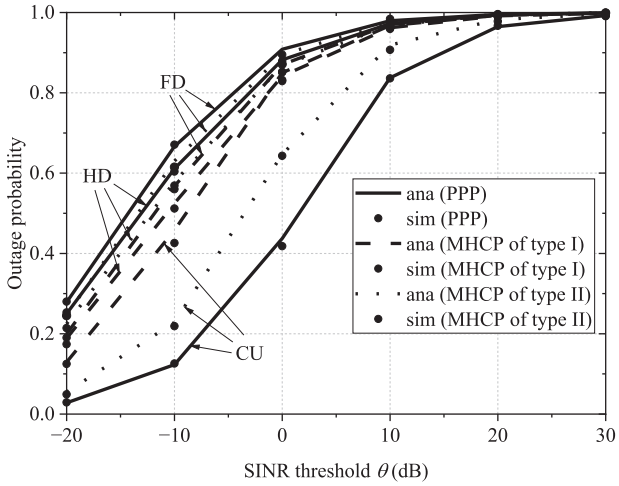

Figure 3: $\mathbb{P}_c$ and $\mathbb{P}_d$ *vs.* θ when BSs follows PPP, MHCP of type I and type II

6.2 Outage Probabilities vs. SINR Threshold in Type II Process

Here, we verify the accuracy of outage probabilities of CUs $\mathbb{P}_c$ and DUs $\mathbb{P}_d$ as the SINR threshold θ varies from -20 to 30 dB, under different settings, i.e., self-interference cancellation factor $\kappa = -50, -70$ dB and noise power $\sigma^2 = -50, -100$ dBm. From Figs. 4a and 4b, we have the following observations:

- Given κ and σ^2, $\mathbb{P}_c$ and $\mathbb{P}_d$ increases as θ increases. The reason is similar with that in Fig. 3 and omitted.
- Given θ, the larger the κ, the larger the $\mathbb{P}_d$ (FD); $\mathbb{P}_d$ (HD) and $\mathbb{P}_c$ remains almost unchanged, as shown in Fig. 4a. Hence, a larger κ means that the FD DU suffers more self-interference[4], and the outage probability of FD DU also increases. However, the outage probabilities of CU and HD DU are not affected.
- Given θ, the larger the σ^2, the larger the $\mathbb{P}_c$ and $\mathbb{P}_d$, as shown in Fig. 4b. It is because a larger σ^2 results in smaller SINRs received at CUs and DUs. With smaller SINRs, we have larger $\mathbb{P}_c$ and $\mathbb{P}_d$, respectively.

6.3 Outage Probabilities vs. Minimum Distance of BSs in Type II Process

Here, we verify the accuracy of outage probabilities of CUs $\mathbb{P}_c$ and DUs $\mathbb{P}_d$ as minimum distance of BSs R_b varies 50 to 300 m, under different settings, i.e., transmission probability of CUs $p_c^t = 0.2$, 0.8, probability of HD DUs $p_H = 0.2, 0.8$. From Figs. 5a and 5b, we have the following observations:

[4]Note that the real ratio value of self-interference cancellation factor κ (in dB [15]) is given by $\kappa = 10^{\kappa/10}$ (no unit [16]). A larger κ means larger self-interference at the FD DU side.

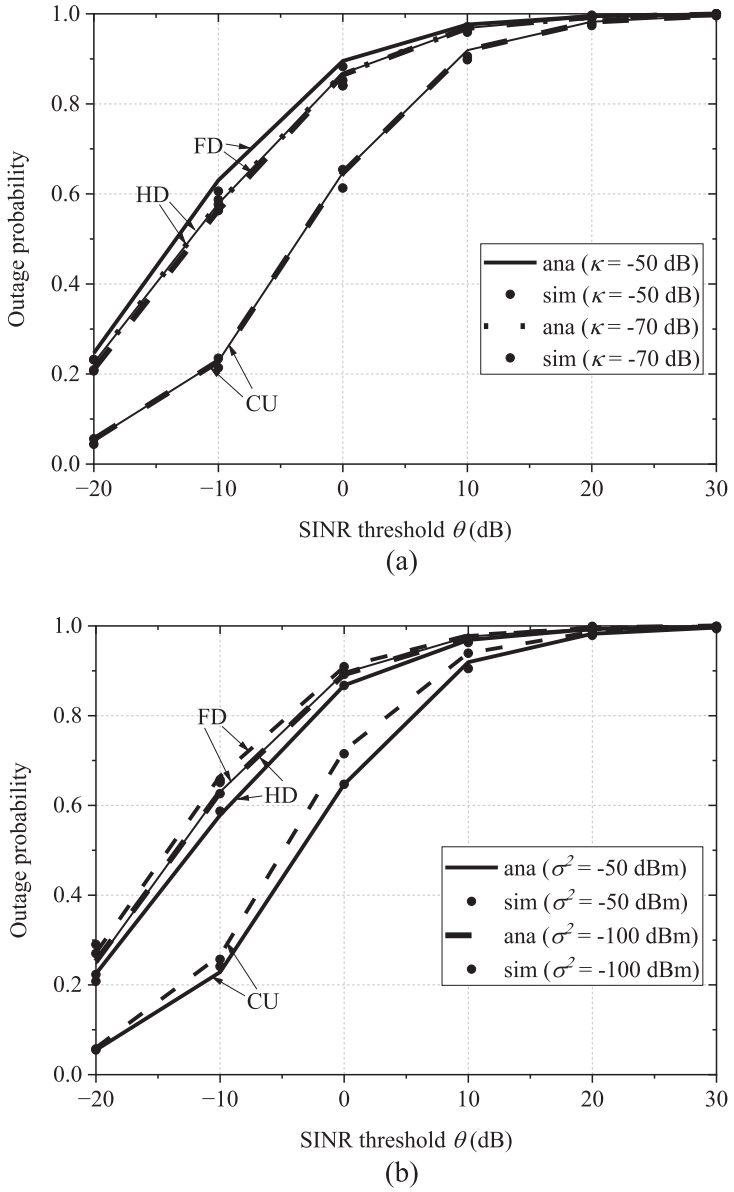

Figure 4: $\mathbb{P}_c$ and $\mathbb{P}_d$ *vs.* θ when (a) $\kappa = -50, -70$ dB and (b) $\sigma^2 = -50, -100$ dBm

- Given p_c^t and p_H, as R_b increases, $\mathbb{P}_d$ decreases while $\mathbb{P}_c$ increases. The reasons are as follows. For DUs, as R_b increases, the intensity of BSs decreases; the intensity of activated DUs increases, the average transmission distance from DU to DU decreases, and the outage probability of DU decreases. For CUs, as R_b increases, the intensity of BSs decreases; the average transmission distance from CU to BS increases, and the outage probability of CU increases.
- Given R_b, the larger p_c^t, the larger the $\mathbb{P}_c$ and $\mathbb{P}_d$, as shown in Fig. 5a. It is because more transmissions from CUs to BSs may bring more mutual interference to the transmissions of CUs and DUs, respectively, and outage probabilities of CUs and DUs also increase.

- Given R_b, the larger p_H, the smaller the $\mathbb{P}_c$ and $\mathbb{P}_d$ (HD), while $\mathbb{P}_d$ (FD) keeps almost unchanged, as shown in Fig. 5b. It is because more HD D2D transmissions result in less FD D2D transmissions, which decrease the interference to the transmissions of CUs and HD DUs, respectively. For FD D2D transmission, the self-interference is dominated among the aggregate interference, hence the outage probability of FD DU is not affected.

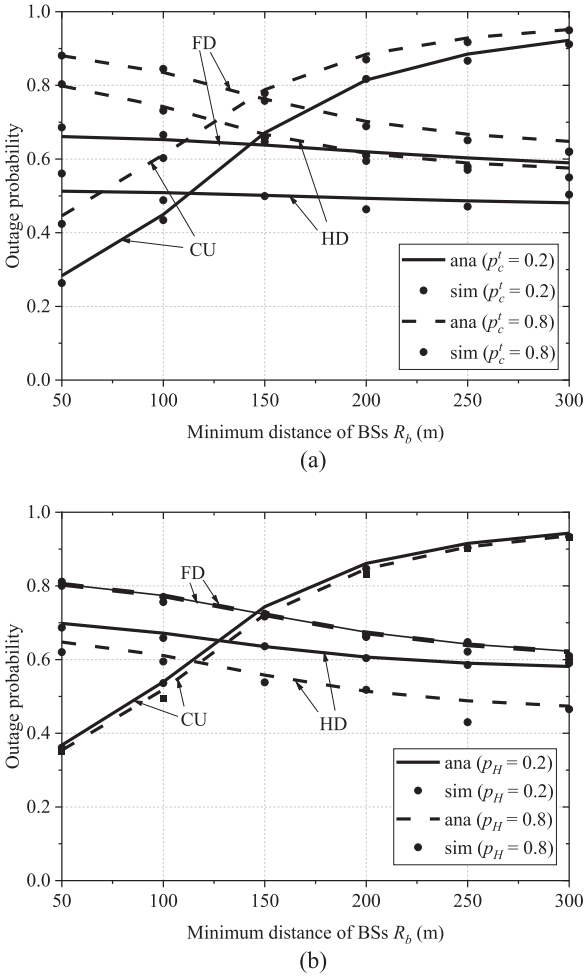

Figure 5: $\mathbb{P}_c$ and $\mathbb{P}_d$ *vs.* d_b when (a) $p_c^t = 0.2, 0.8$; and (b) $p_H = 0.2, 0.8$

6.4 Outage Probabilities vs. Exclusion Zone of BSs in Type II Process

Here, we verify the accuracy of outage probabilities of CUs $\mathbb{P}_c$ and DUs $\mathbb{P}_d$ as the exclusion zone of BSs d_b varies from 0 to 150 m, under different settings, i.e., path-loss exponent $\alpha = 3, 4$, and transmission power of DUs $P_d = 1, 5$ dBm. From Figs. 6a and 6b, we have the following observations:

- Given α and P_d, as d_b increases, $\mathbb{P}_c$ decreases while $\mathbb{P}_d$ increases. The reasons are as follows. As d_b increases, the intensity of activated DUs decreases, the average D2D transmission distance increases, and the outage probability of DU increases; meanwhile, less D2D transmissions may bring less mutual interference to the cellular transmissions, hence the probability of CU decreases.

- Given d_b, the larger the α, the smaller the $\mathbb{P}_c$ and $\mathbb{P}_d$ (HD), the larger $\mathbb{P}_d$ (FD), as shown in Fig. 6a. It is because a larger α means larger power reduction of signals as they propagate through space. For CUs and HD DUs, the interference signals decay more than desired signal for their larger transmission distance. The SINRs received at the CU and HD DU are higher, while $\mathbb{P}_c$ and $\mathbb{P}_d$ (HD) are lower. For FD DUs, the desired signal decays more than self-interference signal for its larger transmission distance. The SINRs received at the FD DU and FD DU are lower, while $\mathbb{P}_d$ (FD) are higher.
- Given d_b, the larger P_d, the smaller the $\mathbb{P}_d$ while the larger $\mathbb{P}_c$, as shown in Fig. 6b. It is because the larger $\mathbb{P}_d$, the larger the received desired signal power at the DU, hence the smaller $\mathbb{P}_d$; in contrast, the larger P_d, the larger the received undesired interference power from DUs at the BS, hence the larger $\mathbb{P}_c$.

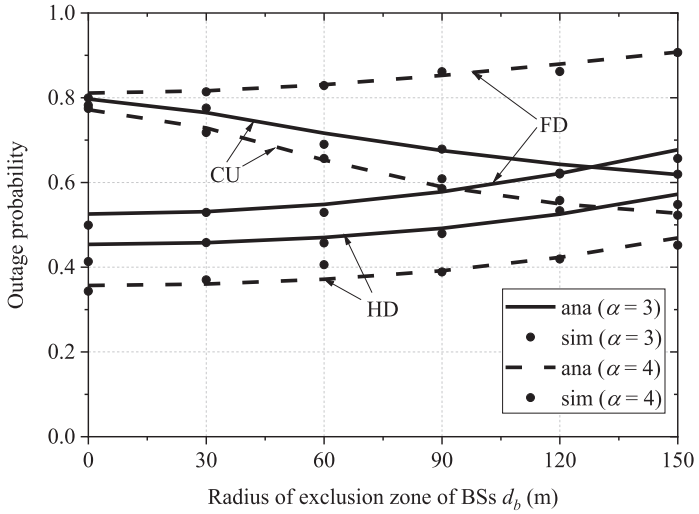

(a)

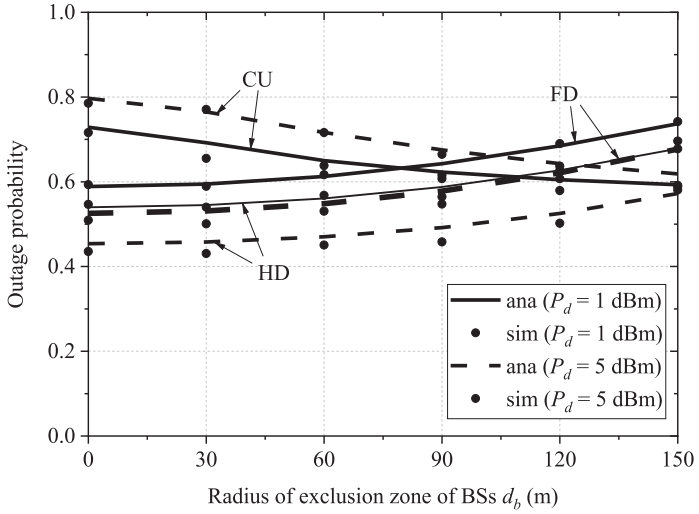

(b)

Figure 6: $\mathbb{P}_c$ and $\mathbb{P}_d$ *vs.* d_b when (a) $\alpha = 3, 4$; (b) $P_d = 1, 5$ dBm

7 Conclusion

Heterogeneous cellular and D2D devices will densely coexist to collect and exchange information and hence have wide application prospects in many fields. To mitigate the interference among the concurrent cellular and D2D transmissions, exclusion zones are set around BS receivers. This paper develops a theoretical model to analyze the outage probabilities of cellular and D2D users in D2D-enabled HetCNets with exclusion zone. It adopts a stochastic geometry approach to model the location randomness of BSs, cellular and D2D devices. Moreover, it captures the randomness and interrelation between cellular and D2D transmissions and characterizes the complex mutual interference among randomly located cellular and D2D devices. Extensive Monte-Carlo simulation results verify that the theoretical model is very accurate.

Acknowledgement: The authors would like to thank the editor and anonymous reviewers for their valuable suggestions and insightful comments, which have greatly improved the overall quality of this paper.

Funding Statement: This work is funded in part by the Science and Technology Development Fund, Macau SAR (Grant Nos. 0093/2022/A2, 0076/2022/A2 and 0008/2022/AGJ), in part by the National Nature Science Foundation of China (Grant No. 61872452), in part by Special fund for Dongguan's Rural Revitalization Strategy in 2021 (Grant No. 20211800400102), in part by Dongguan Special Commissioner Project (Grant No. 20211800500182), in part by Guangdong-Dongguan Joint Fund for Basic and Applied Research of Guangdong Province (Grant No. 2020A1515110162), in part by University Special Fund of Guangdong Provincial Department of Education (Grant No. 2022ZDZX1073).

Author Contributions: The authors confirm contribution to the paper as follows: Yulei Wang: Conceptualization, Methodology, Formal analysis, Software, Validation, Writing–original draft, Writing–review & editing. Li Feng: Conceptualization, Methodology, Writing–review & editing, Supervision, Project administration, Funding acquisition. Shumin Yao: Conceptualization, Methodology, Validation, Writing–review & editing. Hong Liang: Validation, Writing–review & editing. Haoxu Shi: Validation, Writing–review & editing. Yuqiang Chen: Validation, Writing–review & editing. All authors reviewed the results and approved the final version of the manuscript.

Availability of Data and Materials: The data underlying the results presented in the study are available within the article.

Conflicts of Interest: The authors declare that they have no conflicts of interest to report regarding the present study.

References

1. Lin, Z., Li, X., Lau, V. K. N., Gong, Y., Huang, K. (2022). Deploying federated learning in large-scale cellular networks: Spatial convergence analysis. *IEEE Transactions on Wireless Communications, 21(3),* 1542–1556. https://doi.org/10.1109/TWC.2021.3104834
2. Zhang, X., Liu, Y., Liu, J., Argyriou, A., Han, Y. (2021). D2D-assisted federated learning in mobile edge computing networks. *2021 IEEE Wireless Communications and Networking Conference (WCNC)*, Nanjing, China. https://doi.org/10.1109/WCNC49053.2021.9417459
3. Wang, H., Xu, L., Yan, Z., Gulliver, T. A. (2021). Low-complexity MIMO-FBMC sparse channel parameter estimation for industrial big data communications. *IEEE Transactions on Industrial Informatics, 17(5),* 3422–3430. https://doi.org/10.1109/TII.2020.2995598

4. Zhao, Q., Feng, L., Zhao, L., Li, Z., Liang, Y. (2020). SatOpt partition: Dividing throughput-stability region for IEEE 802.11 DCF networks. *IEEE Transactions on Vehicular Technology, 69(9),* 10278–10290. https://doi.org/10.1109/TVT.2020.3004476
5. Zhao, Q., Feng, L., Zhao, L., Xie, K., Liang, Y. (2022). Backoff entropy: Predicting presaturation peak for IEEE 802.11 DCF networks. *IEEE Transactions on Vehicular Technology, 71(2),* 1901–1912. https://doi.org/10.1109/TVT.2021.3131939
6. Liu, X., Xiao, H., Chronopoulos, A. T. (2020). Joint mode selection and power control for interference management in D2D-enabled heterogeneous cellular networks. *IEEE Transactions on Vehicular Technology, 69(9),* 9707–9719. https://doi.org/10.1109/TVT.2020.3001874
7. Shamaei, S., Bayat, S., Hemmatyar, A. M. A. (2019). Interference management in D2D-enabled heterogeneous cellular networks using matching theory. *IEEE Transactions on Mobile Computing, 18(9),* 2091–2102. https://doi.org/10.1109/TMC.2018.2871073
8. Hasan, A., Andrews, J. G. (2007). The guard zone in wireless Ad hoc networks. *IEEE Transactions on Wireless Communications, 6(3),* 897–906. https://doi.org/10.1109/TWC.2007.04793
9. Tefek, U., Lim, T. J. (2016). Interference management through exclusion zones in two-tier cognitive networks. *IEEE Transactions on Wireless Communications, 15(3),* 2292–2302. https://doi.org/10.1109/TWC.2015.2502254
10. Chen, Z., Kountouris, M. (2018). Decentralized opportunistic access for D2D underlaid cellular networks. *IEEE Transactions on Communications, 66(10),* 4842–4853. https://doi.org/10.1109/TCOMM.2018.2834905
11. Chu, M., Liu, A., Chen, J., Lau, V. K. N., Cui, S. (2022). A stochastic geometry analysis for energy-harvesting-based device-to-device communication. *IEEE Internet of Things Journal, 9(2),* 1591–1607. https://doi.org/10.1109/JIOT.2021.3091723
12. Flint, I., Kong, H. B., Privault, N., Wang, P., Niyato, D. (2017). Analysis of heterogeneous wireless networks using poisson hard-core hole process. *IEEE Transactions on Wireless Communications, 16(11),* 7152–7167. https://doi.org/10.1109/TWC.2017.2740387
13. Huang, J., Zou, J., Xing, C. C. (2018). Energy-efficient mode selection for D2D communications in cellular networks. *IEEE Transactions on Cognitive Communications and Networking, 4(4),* 869–882. https://doi.org/10.1109/TCCN.2018.2873004
14. Sun, P., Shin, K. G., Zhang, H., He, L. (2017). Transmit power control for D2D-underlaid cellular networks based on statistical features. *IEEE Transactions on Vehicular Technology, 66(5),* 4110–4119. https://doi.org/10.1109/TVT.2016.2620523
15. Badri, S., Rasti, M. (2021). Interference management and duplex mode selection in in-band full duplex D2D communications: A stochastic geometry approach. *IEEE Transactions on Mobile Computing, 20(6),* 2212–2223. https://doi.org/10.1109/TMC.2020.2977899
16. Ali, K. S., ElSawy, H., Alouini, M. S. (2016). Modeling cellular networks with full-duplex D2D communication: A stochastic geometry approach. *IEEE Transactions on Communications, 64(10),* 4409–4424. https://doi.org/10.1109/TCOMM.2016.2601912
17. Hmamouche, Y., Benjillali, M., Saoudi, S., Yanikomeroglu, H., Renzo, M. D. (2021). New trends in stochastic geometry for wireless networks: A tutorial and survey. *Proceedings of the IEEE, 109(7),* 1200–1252. https://doi.org/10.1109/JPROC.2021.3061778
18. Wang, Y., Zhao, Q., Yao, S., Feng, L., Liang, H. (2022). Performance modeling of tags-to-WiFi transmissions for contention-based WiFi backscatter networks. *2022 IEEE International Conference on Networking, Sensing and Control (ICNSC)*, pp. 1–6. https://doi.org/10.1109/ICNSC55942.2022.10004070
19. Zhang, S., Zhu, Y., Liu, J. (2022). Multi-UAV enabled aerial-ground integrated networks: A stochastic geometry analysis. *IEEE Transactions on Communications, 70(10),* 7040–7054. https://doi.org/10.1109/TCOMM.2022.3204662

20. Okegbile, S. D., Maharaj, B. T., Alfa, A. S. (2021). Interference characterization in underlay cognitive networks with intra-network and inter-network dependence. *IEEE Transactions on Mobile Computing, 20(10),* 2977–2991. https://doi.org/10.1109/TMC.2020.2993408
21. Illian, J., Penttinen, A., Stoyan, H., Stoyan, D. (2008). *Statistical analysis and modelling of spatial point patterns*. England: John Wiley & Sons.
22. Haenggi, M. (2012). *Stochastic geometry for wireless networks*. Cambridge: Cambridge University Press. https://doi.org/10.1017/CBO9781139043816
23. Stoyan, D., Kendall, W. S., Chiu, S. N., Mecke, J. (2013). *Stochastic geometry and its applications*, 3rd edition. England: John Wiley & Sons.
24. Błaszczyszyn, B., Haenggi, M., Keeler, P., Mukherjee, S. (2018). *Stochastic geometry analysis of cellular networks*, 1st edition. Cambridge: Cambridge University Press. https://doi.org/10.1017/9781316677339
25. Ghatak, G., Khosravirad, S. R., Domenico, A. D. (2022). Stochastic geometry framework for ultrareliable cooperative communications with random blockages. *IEEE Internet of Things Journal, 9(7),* 5150–5161. https://doi.org/10.1109/JIOT.2021.3108955
26. ElSawy, H., Hossain, E., Camorlinga, S. (2012). Characterizing random CSMA wireless networks: A stochastic geometry approach. *2012 IEEE International Conference on Communications (ICC)*, pp. 5000–5004. https://doi.org/10.1109/ICC.2012.6363772
27. Ganti, R. K., Haenggi, M. (2006). Regularity in sensor networks. *2006 International Zurich Seminar on Communications*, pp. 186–189. https://doi.org/10.1109/IZS.2006.1649111
28. Chen, H., Liu, L., Dhillon, H. S., Yi, Y. (2019). QoS-aware D2D cellular networks with spatial spectrum sensing: A stochastic geometry view. *IEEE Transactions on Communications, 67(5),* 3651–3664. https://doi.org/10.1109/TCOMM.2018.2889246
29. ElSawy, H., Hossain, E. (2014). On stochastic geometry modeling of cellular uplink transmission with truncated channel inversion power control. *IEEE Transactions on Wireless Communications, 13(8),* 4454–4469. https://doi.org/10.1109/TWC.2014.2316519
30. Liu, Y., Deng, Y., Jiang, N., Elkashlan, M., Nallanathan, A. (2020). Analysis of random access in NB-IoT networks with three coverage enhancement groups: A stochastic geometry approach. *IEEE Transactions on Wireless Communications, 20(1),* 549–564. https://doi.org/10.1109/TWC.2020.3026331
31. Zhang, X., Andrews, J. G. (2015). Downlink cellular network analysis with multi-slope path loss models. *IEEE Transactions on Communications, 63(5),* 1881–1894. https://doi.org/10.1109/TCOMM.2015.2413412
32. Wang, Q., Zhou, Y., Dai, H. N., Zhang, G., Zhang, W. (2022). Performance on cluster backscatter communication networks with coupled interferences. *IEEE Internet of Things Journal, 9(20),* 20282–20294. https://doi.org/10.1109/JIOT.2022.3174002
33. Deng, N., Zhou, W., Haenggi, M. (2015). Heterogeneous cellular network models with dependence. *IEEE Journal on Selected Areas in Communications, 33(10),* 2167–2181. https://doi.org/10.1109/JSAC.2015.2435471
34. Wang, H., Xiao, P., Li, X. (2022). Channel parameter estimation of mmWave MIMO system in urban traffic scene: A training channel-based method. *IEEE Transactions on Intelligent Transportation Systems,* 1–9. https://doi.org/10.1109/TITS.2022.3145363
35. Ma, R., Chang, Y. J., Chen, H. H., Chiu, C. Y. (2017). On relay selection schemes for relay-assisted D2D communications in LTE-A systems. *IEEE Transactions on Vehicular Technology, 66(9),* 8303–8314. https://doi.org/10.1109/TVT.2017.2682123
36. Park, J., Guvenc, I. (2023). Interference analysis for UAV radar networks with guard zones based on stochastic geometry. *IEEE Transactions on Aerospace and Electronic Systems, 59(4),* 4092–4104. https://doi.org/10.1109/TAES.2023.3236308

37. Nguyen, H. Q., Baccelli, F., Kofman, D. (2007). A stochastic geometry analysis of dense IEEE 802.11 networks. *IEEE INFOCOM 2007-26th IEEE International Conference on Computer Communications*, pp. 1199–1207. https://doi.org/10.1109/INFCOM.2007.143
38. Alfano, G., Garetto, M., Leonardi, E. (2011). New insights into the stochastic geometry analysis of dense CSMA networks. *2011 Proceedings IEEE INFOCOM*, pp. 2642–2650. Shanghai, China. https://doi.org/10.1109/INFCOM.2011.5935092
39. Haenggi, M. (2011). Mean interference in hard-core wireless networks. *IEEE Communications Letters, 15(8),* 792–794. https://doi.org/10.1109/LCOMM.2011.061611.110960
40. Deng, N., Wei, H., Haenggi, M. (2023). Modeling and analysis of air-ground integrated networks with flexible beam coverage. *IEEE Transactions on Wireless Communications,* 1. https://doi.org/10.1109/TWC.2023.3260470
41. Andrews, J. G., Baccelli, F., Ganti, R. K. (2011). A tractable approach to coverage and rate in cellular networks. *IEEE Transactions on Communications, 59(11),* 3122–3134. https://doi.org/10.1109/TCOMM.2011.100411.100541
42. Gradshteĭn, I. S., Ryzhik, I. M., Jeffrey, A. (2007). *Table of integrals, series, and products*, 7th edition. London: Academic Press.